A coupled crack initiation and propagation numerical procedure for combined fretting wear and fretting fatigue lifetime assessment

I. Llavori[1,*], A. Zabala[1], M.A. Urchegui[2], W. Tato[1], X. Gómez[1]

[1] *Surface Technologies, Mondragon University, Loramendi 4, 20500 Arrasate-Mondragon, Spain*

[2] *Orona EIC, Orona Ideo, Jauregi bidea s/n, 20120, Hernani, Spain*

Corresponding author: Iñigo Llavori, illavori@mondragon.edu

Abstract. This work presents a numerical procedure for combined fretting wear and fretting fatigue problems. It combines the Archard wear model and the Smith-Watson-Topper fatigue indicator parameter with the Miner damage rule for crack nucleation estimation. The eXtended Finite Element Method (XFEM) is then used in combination with the Archard wear model for crack propagation prediction. This procedure was validated in 12 experimental tests taken from the literature, and a good correlation was found. The procedure allows a detailed study of the interaction between the crack and fretting contact in combination with wear. The results show that the relative slip decreases and changes its distribution unevenly when the crack grows, and highlight the key importance of accounting for wear in order to obtain non-conservative predictions.

Keywords. Fretting wear, fretting, fatigue, numerical analysis

Abbreviations

FEM	=	Finite Element Method
FIP	=	Fatigue Indicator Parameter
FS	=	Fatemi-Socie
LSM	=	Level Set Method
SIF	=	Stress Intensity Factor
SWT	=	Smith-Watson-Topper
TCD	=	Theory of Critical Distances
X-FEM	=	eXtended Finite Element Method

Symbols

a	=	Crack length
b	=	Fatigue strength exponent
b_0	=	Transition crack length from short to long crack propagation regime
C	=	Paris law coefficient
c	=	Fatigue ductility exponent
D	=	Pad diameter
E	=	Young's modulus
$H(\mathbf{x})$	=	Heaviside function
$K_{\mathrm{I}}, K_{\mathrm{II}}, K_{\mathrm{III}}$	=	Stress Intensity Factor mode I, Mode II, and Mode III
K_{IC}	=	Fracture toughness
k	=	Archard wear coefficient
L	=	Critical distance
M	=	Miner's total accumulated damage
m	=	Paris law exponent
$N_{\mathrm{i}}, N_{\mathrm{p}}, N_{\mathrm{f}}$	=	Number of cycles in crack initiation, propagation and failure
n_i	=	Number of cycles completed in each stress state
P, p	=	Contact force, contact pressure
Q	=	Shearing force
R	=	Stress ratio
S_i	=	Shape function
t	=	Time
α	=	Constant related to the compliance of the test rig

ΔK_{th}	=	Threshold Stress Intensity Factor range
$\Delta\sigma_0$	=	Uniaxial plain fatigue limit range
Δh	=	Incremental wear depth
Δn	=	Cycle jump value
Δs	=	Relative slip for a specific point at specific time
δ	=	Relative slip
2Δ	=	Peak to peak displacement
δ_{ext}	=	Displacement measured by the extensometer
$\varepsilon_{\mathrm{f}}^{'}$	=	Fatigue ductility coefficient
$\varepsilon_{\mathrm{n,a}}$	=	Normal strain amplitude
μ	=	Coefficient of friction
$\sigma_{\mathrm{n,max}}$	=	Maximum normal stress,
$\sigma(t)$	=	Cyclic axial stress
σ_{a}	=	Stress amplitude
$\sigma_{\mathrm{f}}^{'}$	=	Fatigue strength coefficient
σ_{y}	=	Yield strength
σ_{u}	=	Tensile strength
υ	=	Poisson coefficient
ϕ,ψ	=	Level set function
Ω	=	Spatial domain
Γ	=	Curve interface

1. - Introduction

Many mechanical components, such as aircraft engine blade housings, ropes, or orthopaedic devices are subjected to fretting wear and fretting fatigue damage. Fretting is the relative movement of a small amplitude between two contacting bodies, which causes damage at the contact surface [1].

In the last few decades, several techniques for fretting fatigue life prediction have been published. Usually the life estimation is divided into two phases, the crack nucleation (N_{i}) and the crack growth (N_{p}) stages, respectively. Therefore, the total life estimation is calculated by the sum of the two stages:

$$N_{\mathrm{f}} = N_{\mathrm{i}} + N_{\mathrm{p}} . \tag{1}$$

On the one hand, the number of cycles for crack nucleation is usually calculated with a Fatigue Indicator Parameter (FIP) such as the Smith-Watson-Topper [2, 3, 4, 5] (SWT) or the Fatemi-Socie [6, 7, 8] (FS). On the other hand, crack propagation cycles are computed using different crack growth laws, such as the well-known Paris law [9].

A coupled crack initiation-propagation methodology requires the definition of two important steps: (i) the stress-strain spot analysis, and (ii) the initial crack length. The most conservative approach is to analyse the crack initiation at the hot-spot [3]. However, a more realistic and less conservative result is obtained when the analysis is performed at a certain distance from the surface [4, 10, 11]. On the other hand, the crack growth stage is typically introduced by a predefined crack length, nevertheless, the selected length is usually arbitrary.

Navarro *et al*. presented a non-arbitrary life estimation methodology [12]. They combined a finite element model to estimate the number of cycles to crack initiation, and an analytical model for the crack propagation stage. Giner *et al.* [8] reported that the use of the eXtended Finite Element Method (X-FEM) for crack growth analysis following the same framework gives a better correlation (about 20% better for crack propagation stage) in fatigue life prediction. The authors attributed these results to the ability of the X-FEM to incorporate the crack-fretting contact interaction effects in the numerical simulation, which cannot be included in analytical solutions.

More recently, the high stress gradient at the trailing edge of the contact motivated the use of non-local methods such as the Theory of Critical Distances [13] (TCD), extensively and successfully used in notch fatigue [14]. This method has been used to define the location for the FIP analysis and the initial crack length [15, 16, 17].

In many cases, fretting fatigue and fretting wear are linked. In order to analyse the effect of wear on fatigue life, Madge *et al*. [18] presented a numerical 2D model that considered material removal. This analysis showed that the SWT parameter value decreases with wear, concluding that the material removal simulation is an essential part of predicting the effect of wear on gross sliding regime. The propagation phase was analysed via a sub-modelling technique with the introduction of a predefined crack length. However, it should be noted that this technique cannot analyse the interaction between the fissure and the fretting contact.

This work presents a coupled wear, crack initiation and propagation methodology in a fully numerical model. The methodology allows to numerically analyse the crack-fretting contact interaction effects during the wear process.

The work is organised as follows. Section 2 first presents a review of the fundamentals of wear, crack initiation and propagation modelling and simulation. The numerical methodology is presented in Section 3, where the flowchart of the numerical architecture is described. In Section 4, the application of the developed procedure is presented, comparing the numerical results with experimental data reported in the literature. Finally, the main conclusions are summarised in Section 5.

2. - Review of wear, crack initiation and propagation modelling and simulation

2.1. – Wear

Many wear description and prediction strategies have been developed based on mechanistic and phenomenological models, and are extensively reviewed in the literature [19, 20, 21, 22]. In this work the phenomenological Archard wear law [22] is used. The Archard local equation [23] is defined as

$$\Delta h(x,t) = \Delta n\, k\, p(x,t)\, \Delta s(x,t), \tag{2}$$

where $\Delta h(x,t)$ is the incremental wear depth, Δn is the cycle jump value, k is the Archard wear coefficient, $p(x,t)$ is the contact pressure, and $\Delta s(x,t)$ is the relative slip for a specific point at specific time.

The wear simulation algorithm used is analogous to the one developed by McColl *et al.* [23] for a two-dimensional numerical model and employed by the present authors [24, 25, 26] for 3D simulations. This process requires high computational costs due to the non-linear nature of the problem, therefore the cycle jump technique is employed [23, 24], which is based on the hypothesis that wear is almost constant over a small number of cycles. In order to ensure a good mesh convergence in wear simulation, a cycle jump of 100 has been selected. Consequently, each simulation cycle represents 100 real cycles.

The implemented wear code, depicted in **Fig. 1**, reads the contact pressure and slip distribution of the contacting nodes in each time increment. Then it calculates the wear depth for each time increment and updates the mesh at the end of the cycle. This approach is slower compared to the methodologies presented by McColl *et al.*[23] or Cruzado *et al.*[25], due to the fact that smaller cycle jumps are required to maintain the convergence of wear simulation. However, it enables successful coupling with the developed crack propagation code, as the information for the cracked elements only needs to be updated once in each cycle.

In order to have a well-defined stress-strain field, a very fine mesh is required in the contact zone. In consequence, the wear depth usually exceeds the length of an element after a few thousand cycles. In this work a multilayer nodes update method [27] has been adopted to account for large wear profiles, as shown in **Fig. 2**.

It should be mentioned that the proposed algorithms would also be applicable to the partial slip regime. In that case, the relative slip displacement calculated to account for wear would be 0 in the sticking zone, therefore, no wear would be applied following Archard's formula (Eq. 2).

2.2. - Crack Initiation

In the last decades different methods for crack initiation estimation have been developed and are extensively reviewed in the literature, such as multiaxial fatigue criteria [18, 28, 29, 30, 31, 32], micromechanics [33, 34], or damage mechanics [35, 36]. In this work, a multiaxial fatigue approach was adopted. Usually, fatigue cracks originate and propagate either in tensile or shear planes [28]. Therefore, it is important to consider at least a shear-based criterion such as the FS, or a normal-based criterion such as the SWT. In fretting cases, shear traction and contact pressure tend toward 0 at the trailing edge of the contact (crack initiation zone), while normal stresses parallel to the surface reach the maximum value (see **Fig. 3**, where analytical solutions are presented for a fretting fatigue partial slip case). Thus, the stresses are close to the uniaxial case, and mode I is predominant. Therefore, this paper employs the SWT multiaxial fatigue criterion [2] (**Eq. 3**) within the critical-plane approach to estimate the location and number of cycles to crack initiation.

$$\mathrm{SWT} = \left(\sigma_{\mathrm{n,max}}\,\varepsilon_{\mathrm{n,a}}\right)_{\max} = \frac{\sigma_{\mathrm{f}}^{'2}}{E}\left(2N_{\mathrm{i}}\right)^{2b} + \sigma_{\mathrm{f}}^{'}\varepsilon_{\mathrm{f}}^{'}\left(2N_{\mathrm{i}}\right)^{b+c}, \tag{3}$$

where $\sigma_{\mathrm{n,max}}$ is the maximum normal stress, $\varepsilon_{\mathrm{n,a}}$ is the normal strain amplitude, $\sigma_{\mathrm{f}}^{'}$ is the fatigue strength coefficient, $\varepsilon_{\mathrm{f}}^{'}$ is the fatigue ductility coefficient, b is the fatigue strength exponent, and c is the fatigue ductility exponent. However, it is important to note that many studies have a good correlation with both criteria [8, 12, 18, 37].

As highlighted in the introduction, a coupled initiation-propagation model requires defining the stress-strain analysis location. It should be mentioned that due to the high stress gradient events in the fretting case, a conservative crack initiation is estimated at the hot-spot. Consequently, a non-local method such as the TCD is recommended. In this work, the l_{opt}-b_{opt} concept developed by Gandiolle and Fouvry [15] based on the TCD has been adopted to set the fatigue analysis location and the initial crack length. Gandiolle and Fouvry found that the optimal incipient crack length (b_{opt}) was equal to the short to long crack propagation regime and the optimal critical distance (l_{opt}) was $l_{\mathrm{opt}} = 0.56 \times b_{\mathrm{opt}}$. This optimal critical distance was very close to the critical distance L defined by Taylor [13] as

$$L = \frac{b_0}{2} = \frac{1}{2\pi}\left(\frac{\Delta K_{\mathrm{th}}}{\Delta\sigma_0}\right)^2, \tag{4}$$

where b_0 is the short to long crack propagation regime considering the Kitagawa-Takahashi formalism [38], ΔK_{th} is the threshold Stress Intensity Factor (SIF) range, and $\Delta\sigma_0$ is the uniaxial plain fatigue limit range for R = -1.

Due to the wear simulation process, the stress-strain field varies in each fretting cycle. The Miner-Palmgrem accumulation rule [39] is therefore used to take into account these different stress-strain states, which is defined as:

$$M = \sum_{i=1}^{k} \frac{n_i}{N_i}, \tag{5}$$

where M is the total accumulated damage (crack is nucleated when M reaches the value of 1), n_i is the number of cycles in each stress state, and N_i is the number of cycles to fracture estimated by the SWT parameter for each stress block cycle. In this paper, the Miner's rule approach previously presented by the authors [25] has been used. As shown in **Fig. 4 (a)**, the centroidal position of the element where the damage is computed changes from cycle to cycle, due to the mesh movement produced by wear simulation. Therefore, the previously accumulated damage is updated to the current centroidal position after each simulated wear cycle, through linear interpolation between elements at different depths (see **Fig. 4 (b)**).

2.3. - Crack Propagation

Crack propagation velocity is usually described in terms of SIFs. Navarro *et al.* [40] analysed several crack growth models related to the fretting fatigue phenomenon. They concluded that the Paris law [9] was one of the best models for the experimental campaign carried out. Accordingly, in this paper the Paris law has been used, which is defined as follows:

$$\frac{\mathrm{d}a}{\mathrm{d}N} = C\left(\Delta K\right)^{m}, \tag{6}$$

where C is the Paris law coefficient, and m is the Paris law exponent.

In the present paper, the computation of the SIFs is calculated with the domain form of the interaction integral code developed by Giner *et al*. [41]. To this end, the numerical simulation of the singular problem is also computed with the X-FEM code developed by the same authors. A detailed implementation of the X-FEM is given in [41], where all the necessary steps and the actual UEL user subroutine code is available. In the present work, it is considered that the crack growth takes place under mode I condition, i.e. straight crack ($\Delta K = K_{\mathrm{I,max}}$). The authors considered the simplification carefully, based on the following analysis:

(i) At the trailing edge of the contact (crack initiation zone) shear and contact stresses tend toward 0, while normal stress parallel to the surface reaches the maximum value (see **Fig. 3**). Thus, the stresses are close to the uniaxial case, and mode I is predominant.

(ii) A previous analysis was performed regarding the crack path orientation. The non-proportional criterion of the maximum amplitude of the normal stress $(\Delta\sigma_{n,eff})_{max}$ proposed by Dubourg and Lamacq [42] predicted a crack path close to vertical direction.

(iii) This simplification (straight crack) has been previously used in fretting literature, reporting good results [8, 12, 43].

(iv) It should be noted that the presented numerical procedure is able to extract SIFs in mixed mode conditions and apply any crack path/orientation criteria, based on fracture mechanics and/or continuum stress field analysis ahead of the crack tip. This assumption is made due to the high computational demand required for simulating a crack bend numerically when wear phenomena are involved. A robust calculation of the SIF values would require a massive decrease in the mesh size, making the simulation too computationally expensive.

The X-FEM presents some advantages over the classical FEM. In the X-FEM [44] the finite element mesh is independent of the crack shape. Additionally, the method does not require cumbersome meshing techniques and a very refined mesh to calculate the stress and strain fields around the crack front. The classical FEM model is enriched with two types of additional degrees of freedom. On the one hand, the discontinuity of the crack faces is described by the Heavisde function ($H(\mathbf{x}) = \pm 1$). On the other hand, the asymptotic behaviour around the crack tip is described by the linear elastic functions defined by Irwin [45]. These functions are given by the following expression:

$$\left\{F^{l}(\mathbf{x})\right\} \equiv \sqrt{r}\left\{\sin\left(\frac{\theta}{2}\right), \cos\left(\frac{\theta}{2}\right), \sin\left(\frac{\theta}{2}\right)\cos(\theta), \cos\left(\frac{\theta}{2}\right)\sin(\theta)\right\}, \tag{7}$$

where r and θ represent the polar coordinates defined with respect to the local reference system at the crack tip. Therefore, the X-FEM approximation to the displacement field is defined as:

$$\mathbf{u}^{\text{X-FEM}}\left(\mathbf{x}\right)=\sum_{i\in I}\mathbf{u}_i S_i\left(\mathbf{x}\right)+\sum_{i\in L}\mathbf{a}_i S_i\left(\mathbf{x}\right)H\left(\mathbf{x}\right)+\sum_{i\in K}N_i\left(\mathbf{x}\right)\left(\sum_{i=1}^{4}\mathbf{b}_i^l F^l\left(\mathbf{x}\right)\right), \tag{8}$$

where I is the set of all nodes in the mesh, L and K are the sets of the enriched nodes, S_i is the shape function, $\mathbf{u}_i$ is the classical degree of freedom of the FEM and $\mathbf{a}_i$ and $\mathbf{b}_i^l$ are the degrees of freedom of the enriched nodes.

An important part of the X-FEM is the geometrical representation of the crack. In this work, the Level Set Method [46] (LSM) has been employed for this task. The LSM is used to discretise a curve into discrete points, where each of these points have a signed distance value. In its general form, the level set ϕ equation can be defined with a time t component as,

$$\phi\left(\mathbf{x},t\right)\begin{cases}>0 & \forall\mathbf{x}\in\Omega^{+},\\ =0 & \forall\mathbf{x}\in\partial\Omega=\Gamma,\\ <0 & \forall\mathbf{x}\in\Omega^{-},\end{cases} \tag{9}$$

where Ω is the interface of interest as shown in **Fig. 5**. Therefore, points outside of the domain have positive values, points inside the domain have negative values, and points on the interface have no sign, as the distance is zero. This version of the LSM is only valid for a closed section.

For an open section, Stolarska *et al.* [47] introduced a modification to the original equation with the use of two level set functions that allowed to track the evolution of open curves such as crack growth problems. The level set ϕ delimitates the two crack surfaces (**Fig. 6 (a)**), while the level set ψ separates the uncracked domain from the crack front (**Fig. 6 (b)**). In case of crack growth problems, the level set functions only need to be defined in a narrow band around the open interface, which lowers the computational cost. Once the level set equations are defined, the enrichment type for the X-FEM simulation is selected (**Fig. 6 (c)**) where each of the enrichments meets the following condition:

$$\text{Heaviside}\quad\begin{cases}\min_{i\in I^{\text{el}}}\left(sign\left(\phi_i\right)\right)\cdot\max_{i\in I^{\text{el}}}\left(sign\left(\phi_i\right)\right)\leq 0,\\ \max_{i\in I^{\text{el}}}\left(sign\left(\psi_i\right)\right)\leq 0,\end{cases} \tag{10}$$

$$\text{Crack tip} \quad \begin{cases} \min_{i\in I^{\mathrm{el}}}\left(sign\left(\phi_i\right)\right)\cdot\max_{i\in I^{\mathrm{el}}}\left(sign\left(\phi_i\right)\right)\leq 0, \\ \min_{i\in I^{\mathrm{el}}}\left(sign\left(\psi_i\right)\right)\cdot\max_{i\in I^{\mathrm{el}}}\left(sign\left(\psi_i\right)\right)< 0. \end{cases} \tag{11}$$

3. – Numerical architecture

This section presents the numerical procedure of the coupled wear, crack initiation and propagation methodology for fretting wear and fatigue. The previously introduced characteristics to be included in the numerical architecture are:

- Wear model
- Fatigue Indicator Parameter
- Damage accumulation rule
- Crack definition by means of the LSM
- X-FEM due to stress singularity around the crack tip
- SIF extraction with domain integrals
- Crack propagation rate criterion

An object-oriented programming approach has been employed due the high number of models and methods needed in the numerical simulation [48]. **Fig. 7** shows the developed code flowchart, which is divided into two large code blocks (the initiation and propagation stages). The crack initiation phase operates under the FEM framework, where the fatigue analysis is iteratively computed during the wear simulation. First, the previously generated Abaqus *inp file is read. This file contains the necessary information to define the mesh, as well as the node and element sets. Next, the numerical analysis corresponding to the first cycle is performed. Once the FEM simulation is completed, a post-process is carried out to compute the incremental wear and the produced damage. This algorithm is repeated until the Miner value is greater than 1. When the damage condition is satisfied, the number of cycles to crack initiation is stored and the first crack segment is generated.

Afterwards, the propagation stage runs under the X-FEM framework. First, the LSM is employed to define the geometrical representation of the crack. It should be highlighted that due to the movement of the mesh to reproduce wear, the LSM algorithm for crack analysis presented by Stolarska *et al*. [47] is not enough, as the information of the level sets defining the crack should be updated. Therefore, for each simulation a complete reanalysis of all crack segments has been carried out in order to define the new position of the nodes with respect to the crack, and to modify the properties of the enriched elements.

Once the enriched elements are defined, the X-FEM simulation is performed. A post-process to compute the incremental wear and to extract the SIFs is carried out, which is then used to calculate the propagation rate. It is noteworthy that with this procedure, the interaction between crack and fretting contact can be analysed in the same numerical model. This algorithm is repeated until the SIF exceeds the critical value. Subsequently the simulation is completed and the estimated crack initiation and propagation cycles are added to compute a total life prediction. It should be highlighted that the number of cycles to be simulated is not determined at the beginning of the numerical analysis, as the simulation finishes when the final failure of the specimen is reached.

4. – Application to fretting wear and fatigue tests

4.1. – Experimental tests used from the literature for comparison

Fretting wear and fatigue experimental tests reported by Magaziner *et al.* [49] were used for numerical model comparisons, the details of which are summarised below. A sketch of the test machine used in these tests, which consists of two servo-hydraulic actuators controlling the alternating axial load (σ), and shearing force (Q), is shown in **Fig. 8**. Therefore, the test machine permits independent control of both loads and is able to control the displacement amplitude of the contacting interfaces.

These tests were performed using a heat-treated and aged titanium alloy Ti-6Al-4V at constant stress amplitude (σ_a = 266 MPa, stress ratio R = 0.03) and a constant maximum contact pressure ($p_{\max}$ = 523 MPa). In each test, the relative displacement (2Δ) was modified in order to analyse the effect of displacement on fretting fatigue lifetime. **Table 1** summarises the test conditions and experimental results selected for the numerical model comparison, and **Table 2** shows the calibration input parameters introduced in the model**.** As far as CoF value is concerned, it should be mentioned at this point that although the CoF in fretting experiments is known to start low and evolve, Sabelkin and Mall [50] suggested that in fretting, a constant CoF of 0.8 for Ti-6Al-4V could be a representative value for the entire test.

The descriptions reported in [53] were followed for the fretting loop definition. Digitalised loops from the experimental test number 6A at different stages are depicted in **Fig. 9 (a)** and **Fig. 9 (b)**, corresponding to 1,000 and 40,000 cycles respectively.

Fig. 9 (a) shows the relative displacement between bodies (peak to peak displacement, 2Δ) and the contact slip (2δ), which is smaller than the relative displacement. It can be observed that the relative contact slip at 40,000 cycles (**Fig. 9 (b)**) decreases drastically compared to the 1,000-cycle loop (**Fig. 9 (a)**).

4.2. – Finite element modelling

The model shown in **Fig. 10** has been developed in the commercial code Abaqus FEA. Due the symmetry of the cylinder on the flat fretting fatigue test configuration, half of the specimens have been modelled as in references [7, 8, 18, 36]. The model consists of linear quadrilateral elements of four nodes (CPE4, plane strain), with further refinement on the contact interface by the partition technique**.** The element depth at the contact area is 20 μm, consequently the fatigue analysis location has been changed from the target (9 μm, $l_{\mathrm{opt}} = 0.56 \times b_{\mathrm{opt}}$) to the centroid of the element (where the damage is monitored, at 10 μm) for convenience. An initial crack length of 16 μm (b_{opt}=b_0) was considered.

In order to obtain a precise slip distribution, the Coulomb and the Lagrange multiplier methods have been used to model the tangential contact. A linear elastic model was used as material model, since the experiments were carried out in the elastic regime (this assumption was validated in [18]).

Fig. 11 and **Fig. 12** show the load cycle history which has been divided into three steps. In the first step, a normal load P is applied followed by a bulk load σ and a prescribed displacement δ_{app} in order to accommodate the contacting interface. It should be mentioned that multipoint constraint technique (MPC) has been employed in order to apply the contact force (P) and the remote stress (σ). Finally, a cyclic bulk load $\sigma(t)$ and displacement $\delta_{\mathrm{app}}(t)$ are applied simultaneously. The prescribed slip for each test has been calculated from the displacement described in the experiments [49], through the equations (12, 13 and 14) proposed by Wittkowsky *et al.* [54],

$$\Delta = \delta_{\mathrm{AB}} - \left(\delta_{\mathrm{ext}} + \delta_{\mathrm{DC}}\right), \tag{12}$$

$$\delta_{\mathrm{AB}} = \frac{F-2Q}{AE} l_{\mathrm{AB}}, \tag{13}$$

$$\delta_{\mathrm{DC}} = -\alpha l_{\mathrm{DC}} Q, \tag{14}$$

where δ_{AB} is the relative displacement between A and B (see **Fig. 8**), δ_{ext} is the displacement measured by the extensometer, δ_{DC} is the displacement due to the compliance of the fretting configuration system, l_{AB} is the distance between A and B, l_{DC} is the distance between C and D, A is the cross-section area of the specimen, and α is the constant that is related to the compliance. The available data to calculate δ_{ext} (which is the applied displacement in the numerical simulations, *i.e.* δ_{app}) can be found in [49].

4.3. - Contact stresses and SIF validation against analytical solutions

An important step in any numerical simulation is to check the model against benchmark solutions. In this case, in order to check the accuracy of the simulation, the contact stresses of an unworn finite element model [55] have been compared to an analytical formulation [56] for a fretting fatigue case in a partial slip regime. The magnitude of the applied displacement on the pad (**Fig. 10**) has been calibrated to match the desired shear load. **Fig. 13** shows that the numerical model simulation is in very good agreement with the analytical solution for contact pressure (**Fig. 13 (a)**), shear traction (**Fig. 13 (b)**) and normal stress parallel to the surface (**Fig. 13 (c)**).

On the other hand, the extraction of the SIF has been compared to benchmark problems, such as SENT, DENT, and centred crack (**Fig. 14**), where analytical equations are readily available [57]. In this case, the numerical results have been compared to the weight function method (a_c = 1mm, w = 4 mm, σ = 1 MPa). As shown in Table 3, numerical predictions are in very good agreement with the theoretical results (differences below 0.2 %).

Additionally, it should be mentioned that this X-FEM implementation has also been tested for a mixed mode Westergaard's crack problem with very high accuracy compared to the exact solution [41].

4.4. – Numerical results, lifetime prediction, and correlation with experimental tests

Fig. 15 shows the damage evolution estimation up to crack initiation, corresponding to tests with a low and high relative contact slip (test 9A and 10A respectively). In order to evaluate the importance of wear simulation on fatigue life prediction, analyses with and without considering wear phenomena were conducted. As can be observed, the Miner parameter reaches the value of 1 for both tests when wear is not computed. Conversely, the behaviour differs when wear is calculated, which is consistent with experimental observation. Test 10A reaches a maximum value of 0.2 at 3,000 cycles and remains constant with a slight downward tendency, while test 9A shows that wear phenomena enlarge the crack initiation process, delaying the predicted crack nucleation time. This phenomenon is attributed to the fact that the damage is removed by the wear process delaying the crack initiation. Consequently, the need for computing wear in order to obtain a non-conservative life estimation should be highlighted.

The coupled nature of the presented simulation allows to analyse the interaction between the crack growth and wear. **Fig. 16** shows the evolution of the contact slip range and the distribution of the von Mises stress field at different stages on the simulation corresponding to test 9A, which reached the final fracture. It can be observed that at the start of the simulation (**Fig. 16 (a)**), the slip distribution at each contact node is around 6-10 μm. The contact area grows incrementally due to wear simulation prior to the crack initiation (10,000 cycles), and a discontinuity of the slip distribution is observed once the crack is generated (20,000 and 30,000 cycles). This behaviour is exacerbated prior to the rupture of the specimen (**Fig. 16 (b)** from 40,000 cycles onward), where the contact slip is reduced drastically at the left side of the crack lip. This is associated with the loss of stiffness produced by the crack [58], which avoids the full transmission of the bulk stress to the left side of the contact, as can be observed in the von Mises stress field (**Fig. 16 (d)**). This observation is in a good agreement with the experimental results. As can be observed in the previously introduced **Fig. 9**, the experimental loops show a decrease of the relative contact slip along the test.

Table 4 and **Fig. 17** show the comparison between the predicted lifetime (Num. N_f) and the experimental result (Exp. N_f) for each test. It should be mentioned that in these tests, a broad range of conditions with different slip amplitudes (ranging from 27-260 μm), contact forces (between 400-4003 N) and pad radii (ranging from 5.08-50.08 mm) were used (see **Table 1**). Taking into account that fatigue is characterised with a high scatter of lifetime, the predictions obtained by the proposed methodology are relatively close to the experimental lives, with a mean error value of 33% for the tests 1A-9A (all error values are below 53.5 %). **Some good examples that show the same trends in fretting fatigue can be found in [8, 12].** Additionally, in the tests corresponding to the largest slip amplitudes (10A-12A) the simulation did not predict the failure of the specimen, which correlates with the experimental test, as the samples did not fail when the maximum number of cycles (10^6) was reached. Therefore, the numerical results seem to be in good agreement with the experimental data.

5. – Conclusions

In this work the following conclusions can be drawn from the obtained results:

- A 2D cylinder on flat numerical architecture that combines wear, crack initiation and crack propagation has been successfully implemented, obtaining a good correlation with a broad range of different configurations in terms of slip amplitudes, contact forces, and pad radii. The key novelty of this numerical model is that it explicitly simulates wear and crack propagation simultaneously.
- The numerical results show that the relative slip in the contact zone decreases when the crack length grows due to the loss of local stiffness produced by the crack. This observation is in a good agreement with the experimental results.
- The coupled simulation allowed to observe that the interaction of the crack growth and fretting contact affects the slip distribution unevenly at each side of the crack lip, significantly affecting wear evolution.
- The generated damage is removed during the wear process, delaying the onset of a crack which leads to a prediction of higher life expectancy compared to simulations that do not account for wear. The implementation of wear is therefore a key factor in order to compute more representative and less conservative life estimations.

- The results obtained suggest that the proposed procedure might be used to estimate combined fretting fatigue and fretting wear lives, and can potentially be applied to more complex geometries.

Acknowledgements

The authors gratefully acknowledge the financial support given by the Basque Government under the "Proyectos de Investigacion Básica y/o Aplicada" (Project NUSIMCO: Ref.PI2013-23), and "Programa de apoyo a la investigación colaborativa en áreas estratégicas" (Project MEDECA: Ref. KK-2017/00053, and MEDECA2: Ref. KK-2018/00013) programs.

References

[1] O. Vingsbo and S. Soderberg, "On fretting maps," *Wear*, vol. 126, pp. 131–147, 1988.

[2] R. Smith, P. Watson, and T. Topper, "A stress-strain function for the fatigue of metals," *Journal of Material*, vol. 5, no. 4, pp. 767–778, 1970.

[3] M. Szolwinski and T. Farris, "Observation, analysis and prediction of fretting fatigue in 2024-t351 aluminum alloy," *Wear*, vol. 221, no. 1, pp. 24–36, 1998.

[4] W. Sum, E. Williams, and S. Leen, "Finite element, critical-plane, fatigue life prediction of simple and complex contact configurations," *International Journal of Fatigue*, vol. 27, no. 4, pp. 403–416, 2005.

[5] A. Belloula, A. Amrouche, M. Nait-Abdelaziz, and N. Benseddiq, "Comparison of the cracking energy density and the smith–watson–topper parameters in predicting fretting fatigue lifetime of a steel/aluminum alloy contact," *Fatigue & Fracture of Engineering Materials & Structures*, vol. 37, no. 12, pp. 1355–1366, 2014.

[6] A. Fatemi and D. Socie, "A critical plane approach to multiaxial fatigue damage including out-of-phase loading," *Fatigue & Fracture of Engineering Materials & Structures*, vol. 11, no. 3, pp. 149–165, 1988.

[7] C. Navarro, S. Muñoz, and J. Dominguez, “On the use of multiaxial fatigue criteria for fretting fatigue life assessment,” *International Journal of fatigue*, vol. 30, pp. 32–44, 2008.

[8] E. Giner, C. Navarro, M. Sabsabi, M. Tur, J. Domnguez, and F. Fuenmayor, “Fretting fatigue life prediction using the extended finite element method,” *Ínternational Journal of Mechanical Sciences*, vol. 53, no. 3, pp. 217–225, 2011.

[9] P. Paris and F. Erdogan, “A critical analysis of crack propagation laws,” ASME, 1963.

[10] J. Madge, S. Leen, I. McColl, and P. Shipway, “Contact-evolution based prediction of fretting fatigue life: effect of slip amplitude,” *Wear*, vol. 262, no. 9, pp. 1159–1170, 2007.

[11] D. Houghton, P. Wavish, E. Williams, and S. Leen, “Multiaxial fretting fatigue testing and prediction for splined couplings,” *International Journal of Fatigue*, vol. 31, no. 11, pp. 1805–1815, 2009.

[12] C. Navarro, J. Vázquez, and J. Dominguez, “A general model to estimate life in notches and fretting fatigue,” *Engineering Fracture Mechanics*, vol. 78, no. 8, pp. 1590–1601, 2011.

[13] D. Taylor, *The theory of critical distances: a new perspective in fracture mechanics*. Elsevier, 2010.

[14] L. Susmel, *Multiaxial notch fatigue*. Elsevier, 2009.

[15] C. Gandiolle and S. Fouvry, “Stability of critical distance approach to predict fretting fatigue cracking: a l opt–b opt concept,” *International Journal of Fatigue*, vol. 82, pp. 199–210, 2016.

[16] J. Araújo, L. Susmel, M. Pires, and F. Castro, “A multiaxial stress-based critical distance methodology to estimate fretting fatigue life,” *Tribology International*, vol. 108, pp. 2–6, 2017.

[17] M. Nesládek, M. Španiel, J. Kuželka, J. Jurenka, and K. Doubrava, “A fretting damage correction factor applicable to the mcdiarmid criterion of plain high-cycle fatigue,” *Fatigue & Fracture of Engineering Materials & Structures*, vol. 40, no. 1, pp. 27–44, 2017.

[18] J. Madge, S. Leen, and P. Shipway, “A combined wear and crack nucleation–propagation methodology for fretting fatigue prediction,” *International Journal of Fatigue*, vol. 30, no. 9, pp. 1509–1528, 2008.

[19] H. Meng and K. Ludema, “Wear models and predictive equations: their form and content,” *Wear*, vol. 181, pp. 443–457, 1995.

[20] S. Hsu, M. Shen, and A. Ruff, “Wear prediction for metals,” *Tribology International*, vol. 30, no. 5, pp. 377–383, 1997.

[21] P. Blau, “Fifty years of research on the wear of metals,” *Tribology*, vol. 30, no. 5, pp. 321–331, 1997.

[22] J. Archard and H. W, “The wear under unlubricated conditions,” in *Proceedings of the Royal Society of London. Series A*, vol. 236, pp. 397–410, 1956.

[23] I. McColl, J. Ding, and S. Leen, “Finite element simulation and experimental validation of fretting wear,” *Wear*, vol. 256, pp. 1114–1127, 2004.

[24] A. Cruzado, M. Urchegui, and X. Gómez, “Finite element modeling and experimental validation of fretting wear scars in thin steel wires,” *Wear*, vol. 289, pp. 26–38, 2012.

[25] A. Cruzado, S. Leen, M. Urchegui, and X. Gómez, “Finite element simulation of fretting wear and fatigue in thin steel wires,” *International Journal of Fatigue*, vol. 55, pp. 7–21, 2013.

[26] A. Cruzado, M. Urchegui, and X. Gómez, “Finite element modeling of fretting wear scars in the thin steel wires: Application in crossed cylinder arrangements,” *Wear*, vol. 318, no. 1-2, pp. 98–105, 2014.

[27] L. Tang, S. Ding, Y. Xie, and Y. Huo, “A multilayer nodes update method in fem simulation of large depth fretting wear,” *Wear*, vol. 301, no. 1, pp. 483–490, 2013.

[28] D. Socie and G. Marquis, *Multiaxial Fatigue*. SAE, 2000.

[29] C. Lykins, S. Mall, and V. Jain, “A shear stress-based parameter for fretting fatigue crack initiation,” *Fatigue & Fracture of Engineering Materials & Structures*, vol. 24, no. 7, pp. 461–473, 2001.

[30] E. Mamiya, F. Castro, and J. Araújo, "Recent developments on multiaxial fatigue: The contribution of the university of braslia," *Theoretical and Applied Fracture Mechanics*, vol. 73, pp. 48–59, 2014.

[31] J. Vázquez, C. Navarro, and J. Domnguez, "A model to predict fretting fatigue life including residual stresses," *Theoretical and Applied Fracture Mechanics*, vol. 73, pp. 144–151, 2014.

[32] R. H. Talemi, "Numerical measures of non-proportionality degree in incomplete contact subjected to fretting fatigue loading," *Theoretical and Applied Fracture Mechanics*, vol. 90, pp. 33–42, 2017.

[33] D. McDowell and F. Dunne, "Microstructure-sensitive computational modeling of fatigue crack formation," *International journal of fatigue*, vol. 32, no. 9, pp. 1521–1542, 2010.

[34] O. McCarthy, J. McGarry, and S. Leen, "Micro-mechanical modelling of fretting fatigue crack initiation and wear in ti–6al–4v," *International Journal of Fatigue*, vol. 62, pp. 180–193, 2014.

[35] T. Zhang, P. McHugh, and S. Leen, "Finite element implementation of multiaxial continuum damage mechanics for plain and fretting fatigue," *International Journal of Fatigue*, vol. 44, pp. 260–272, 2012.

[36] R. Hojjati-Talemi and M. Wahab, "Fretting fatigue crack initiation lifetime predictor tool: using damage mechanics approach," *Tribology International*, vol. 60, pp. 176–186, 2013.

[37] S. O´Halloran, P. Shipway, A. Connaire, S. B. Leen, and A. Harte, "A combined wear-fatigue design methodology for fretting in the pressure armour layer of flexible marine risers," *Tribology International*, vol. 108, pp. 7–15, 2017.

[38] H. Kitagawa and S. Takahashi, "Applicability of fracture mechanics to very small cracks or the cracks in the early stage," in *Second International Conference on Mechanical Behavior of Materials. ASM, Metals Park, Ohio. 1976, 627-631*, 1976.

[39] M. Miner, "Cumulative damage in fatigue," *Journal of Applied Mechanics*, vol. 12, no. 3, pp. A159–A164, 1945.

[40] C. Navarro, S. Muñoz, and J. Dominguez, "Propagation in fretting fatigue from a surface defect," *Tribology international*, vol. 39, no. 10, pp. 1149–1157, 2006.

[41] E. Giner, N. Sukumar, T. Tarancon, and F. Fuenmayor, "An abaqus implementation of the extended finite element method," *Engineering fracture mechanics*, vol. 76, pp. 347–368, 2009.

[42] M.-C. Dubourg and V. Lamacq, "Stage ii crack propagation direction determination under fretting fatigue loading: a new approach in accordance with experimental observations," in *Fretting fatigue: current technology and practices*, ASTM International, 2000.

[43] O. J. McCarthy, J. McGarry, and S. B. Leen, "Microstructure-sensitive prediction and experimental validation of fretting fatigue," *Wear*, vol. 305, no. 1-2, pp. 100–114, 2013.

[44] M. Moes, J. Dolbow, and T. Belytschko, "A finite element method for crack growth without remeshing," *International journal for numerical methods in engineering*, vol. 46, no. 1, pp. 131–150, 1999.

[45] G. Irwin, "Analysis of stresses and strains near the end of a crack traversing a plate," *Journal of applied mechanics*, vol. 24, no. 3, pp. 361–364, 1957.

[46] S. Osher and J. Sethian, "Fronts propagating with curvature-dependent speed: algorithms based on hamilton-jacobi formulations," *Journal of computational physics*, vol. 79, no. 1, pp. 12–49, 1988.

[47] M. Stolarska, D. Chopp, N. Moës, and T. Belytschko, "Modelling crack growth by level sets in the extended finite element method," *International journal for numerical methods in Engineering*, vol. 51, no. 8, pp. 943–960, 2001.

[48] J. Rumbaugh, M. Blaha, W. Premerlani, F. Eddy, and W. E. Lorensen, *Object-oriented modeling and design*, vol. 199. Prentice-hall Englewood Cliffs, NJ, 1991.

[49] R. Magaziner, O. Jin, and S. Mall, "Slip regime explanation of observed size effects in fretting," *Wear*, vol. 257, no. 1-2, pp. 190–197, 2004.

[50] V. Sabelkin and S. Mall, "Relative slip on contact surface under partial slip fretting fatigue condition," *Strain*, vol. 42, no. 1, pp. 11–20, 2006.

[51] N. Dowling, *Mechanical behavior of materials: engineering methods for deformation, fracture, and fatigue*. Pearson, 2012.

[52] C. EduPack, "Granta design ltd," *Cambridge UK (www.grantadesign.com/education)*, 2016.

[53] S. Pearson and P. Shipway, "Is the wear coefficient dependent upon slip amplitude in fretting? vingsbo and söderberg revisited," *Wear*, vol. 330, pp. 93–102, 2015.

[54] B. Wittkowsky, P. Birch, J. Dominguez, and S. Suresh, "An apparatus for quantitative fretting fatigue testing," *Fatigue Fract. Eng. Mater. Struct*, vol. 22, no. 4, pp. 307–320, 1999.

[55] R. Hojjati-Talemi, M. A. Wahab, J. De Pauw, and P. De Baets, "Prediction of fretting fatigue crack initiation and propagation lifetime for cylindrical contact configuration," *Tribology International*, vol. 76, pp. 73–91, 2014.

[56] J. Vázquez, C. Navarro, and J. Domnguez, "A new method for obtaining the stress field in plane contacts," *Ínternational Journal of Solids and Structures*, vol. 49, no. 26, pp. 3659–3665, 2012.

[57] T. Fett and D. Munz, *Stress intensity factors and weight functions*, vol. 1. Computational Mechanics, 1997.

[58] E. Giner, M. Tur, A. Vercher, and F. Fuenmayor, "Numerical modelling of crack–contact interaction in 2d incomplete fretting contacts using x-fem," *Tribology International*, vol. 42, no. 9, pp. 1269–1275, 2009.

Figures

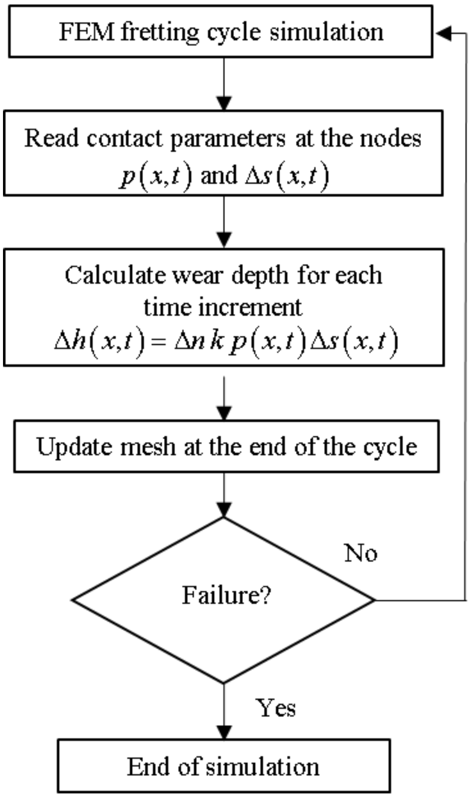

Fig. 1.Adopted wear methodology algorithm.

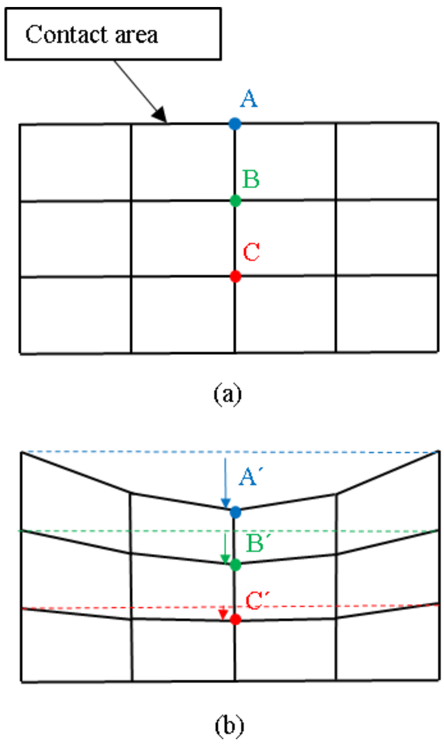

Fig. 2. The multilayer nodes update method [27] adopted in this work. (a): unworn geometry, (b): updated coordinates for all nodes under the contact area.

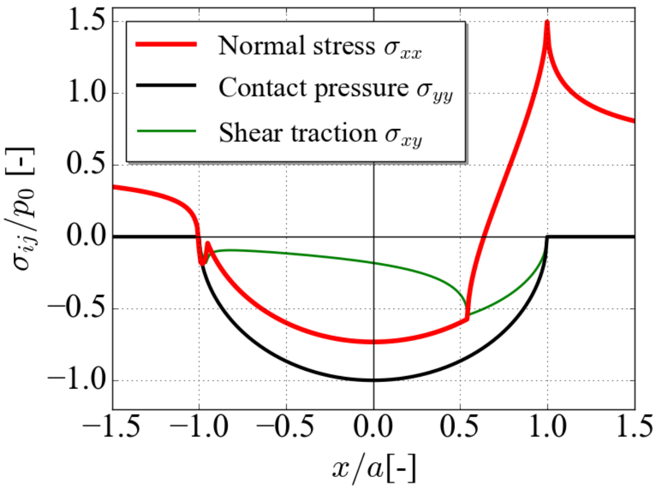

Fig. 3. Analytic solution for normal stress parallel to the surface, shear traction and contact pressure.

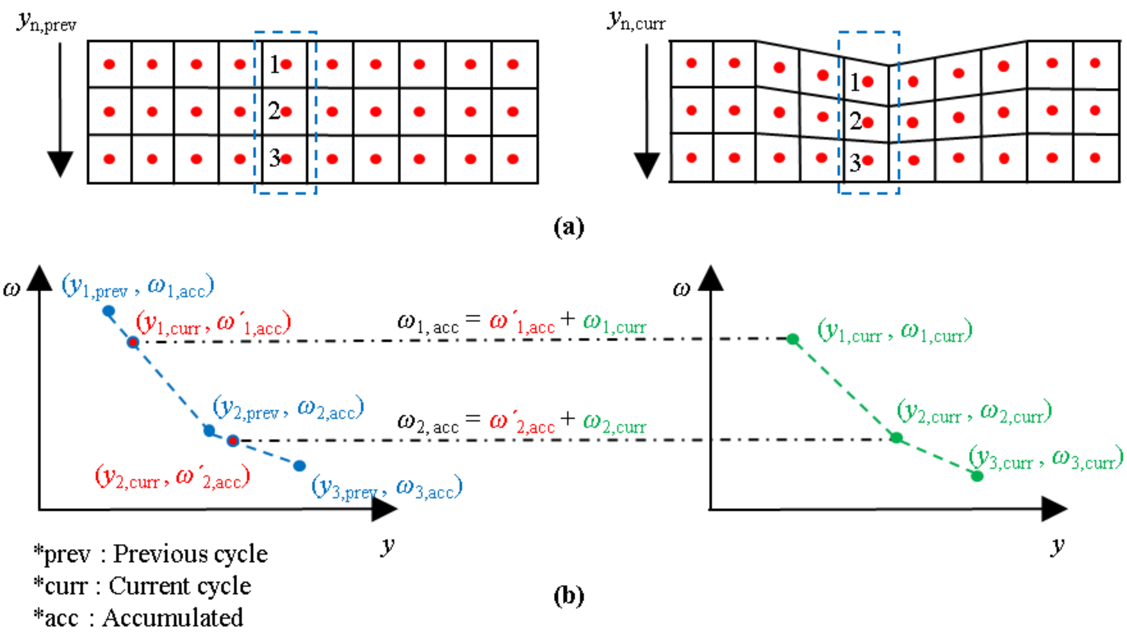

Fig. 4. Damage accumulation framework developed by the authors [25]. (a): Schematic view of the movement of the centroidal position of the elements due to wear simulation. (b): Damage update scheme through linear interpolation between elements at different depths.

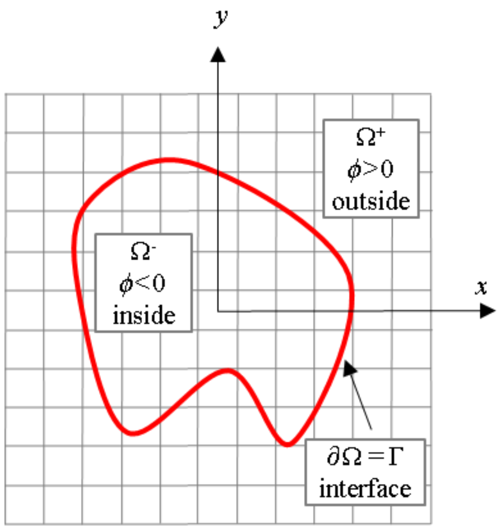

Fig. 5. Example of a level set function for a closed domain.

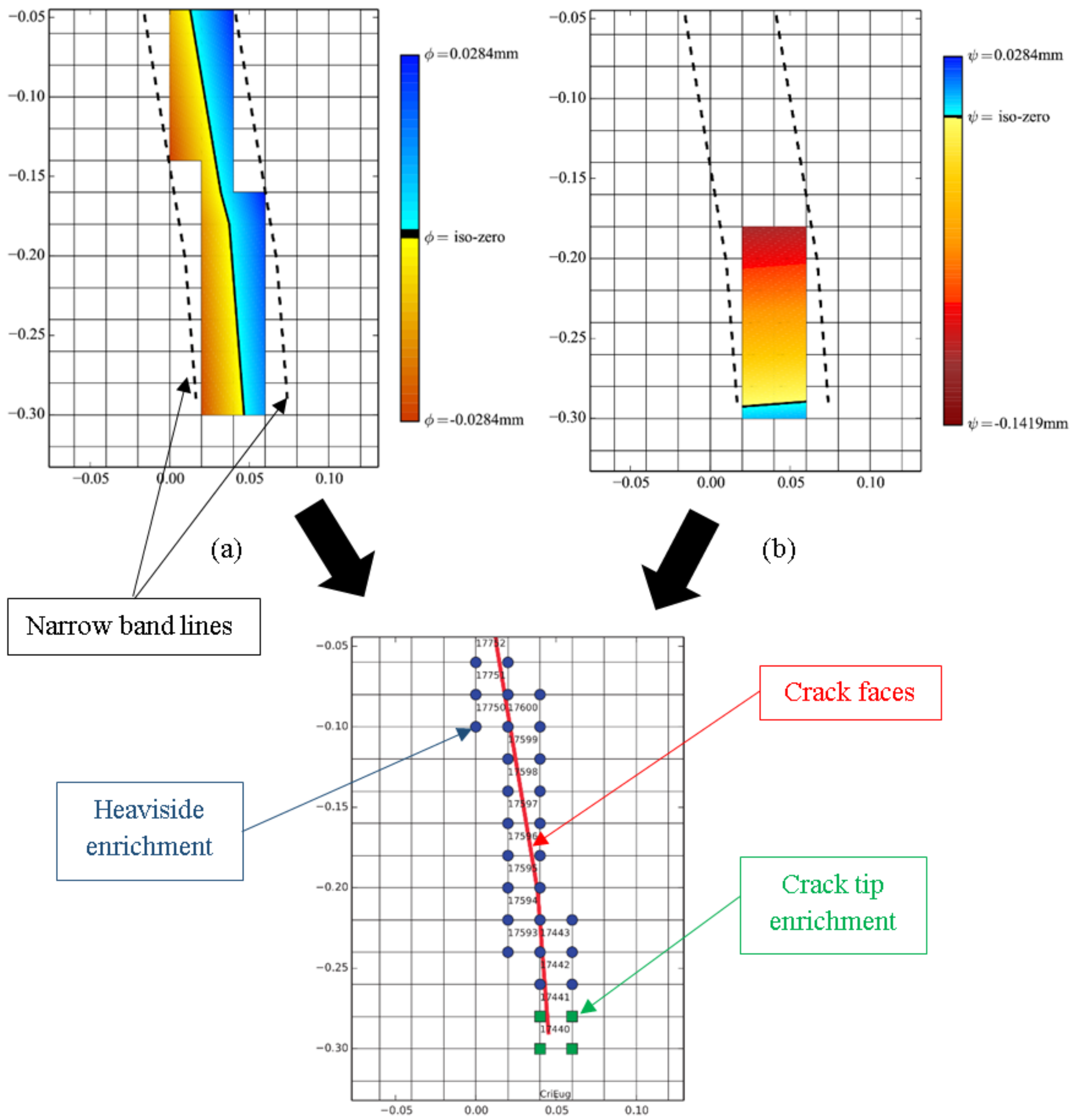

Fig. 6. Geometrical crack representation by means of the narrow band LSM: (a) LS ϕ that defines the crack faces; (b) LS ψ that defines the crack front; (c) Heaviside and crack tip enriched elements defined by the LSM.

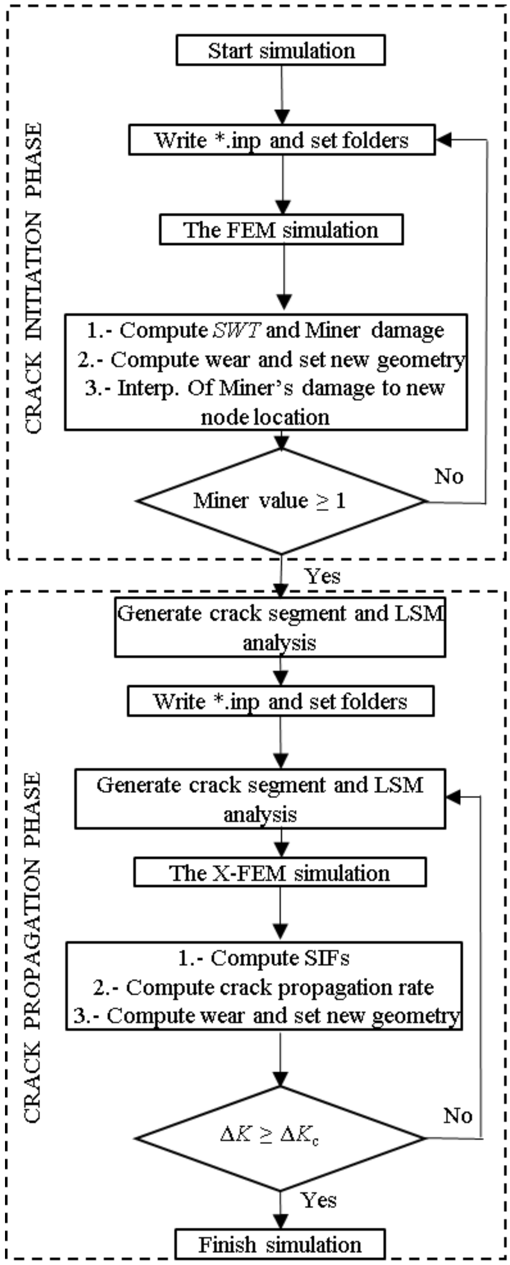

Fig. 7.Flow chart computational sequence for numerical analysis.

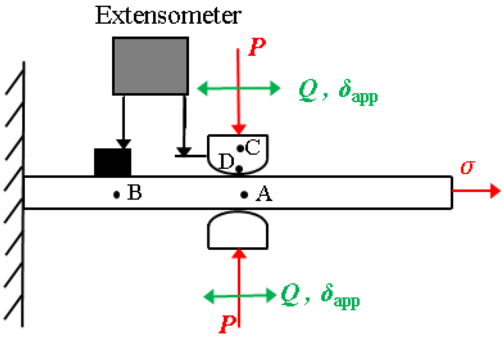

Fig. 8. Sketch of the test machine reported by Magaziner *et al.* [49].

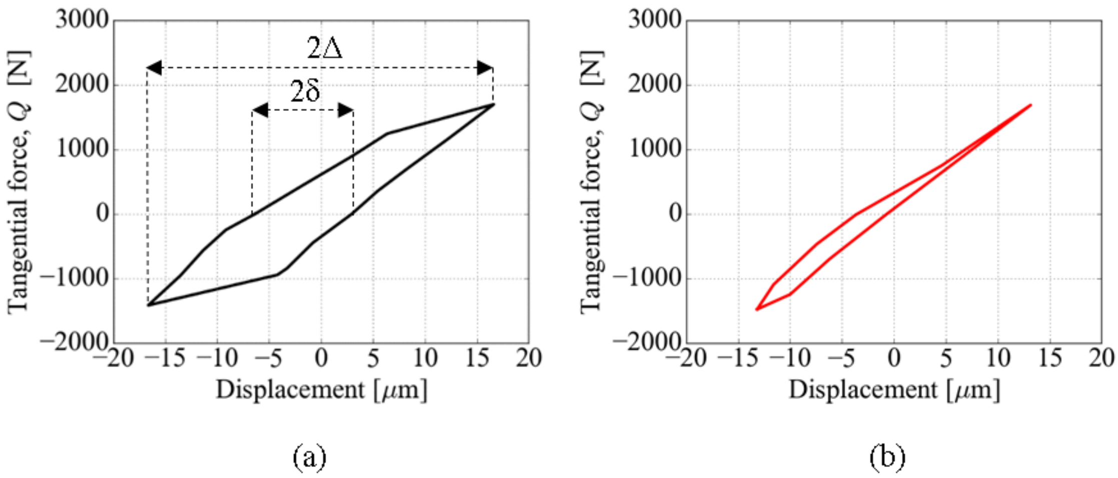

Fig. 9. Fretting loop at different stages of test 6A. The hysteresis loops were digitalised from reference [49]: (a) fretting loop from cycle 1,000; (b) fretting loop from cycle 40,000.

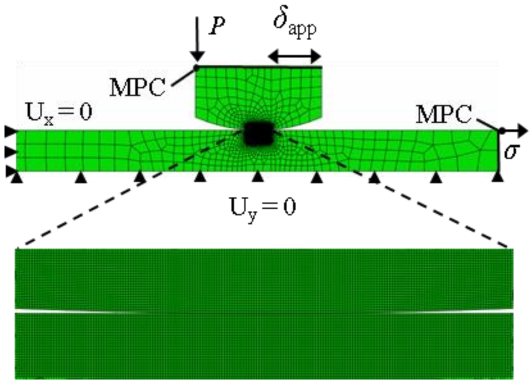

Fig. 10. Geometry, mesh, and applied boundary condition and forces of the numerical models.

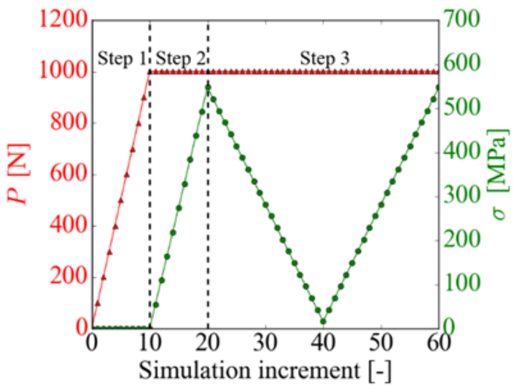

Fig. 11. FEA steps: Normal (triangles) and bulk (dots) loads.

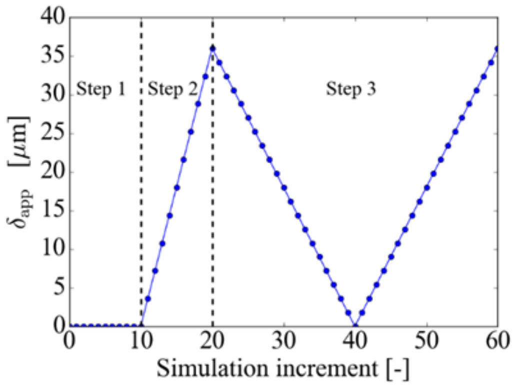

Fig. 12. FEA steps: Applied displacement δ_{app} .

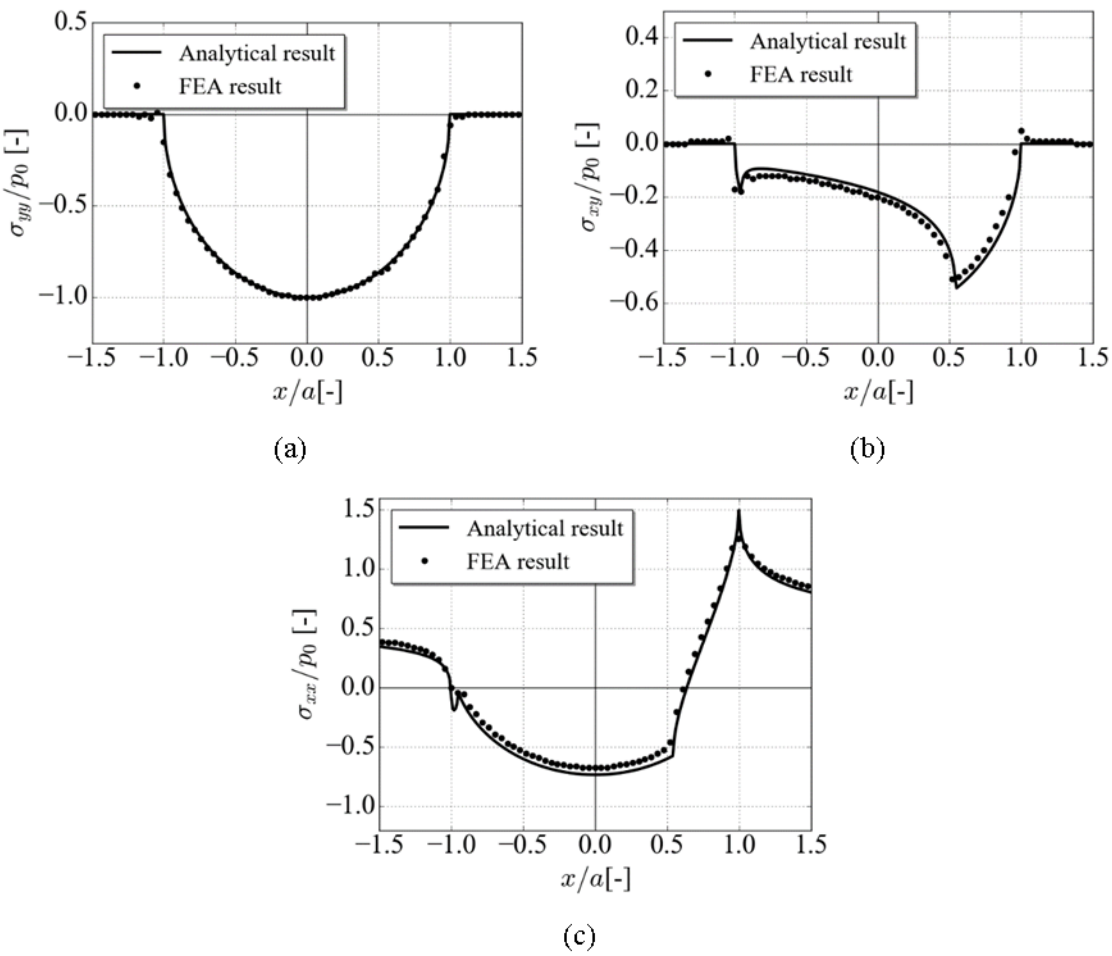

Fig. 13. Comparison between FEA results and an analytical solution. (a) Contact pressure; (b) shear traction; (c) normal stress parallel to the surface.

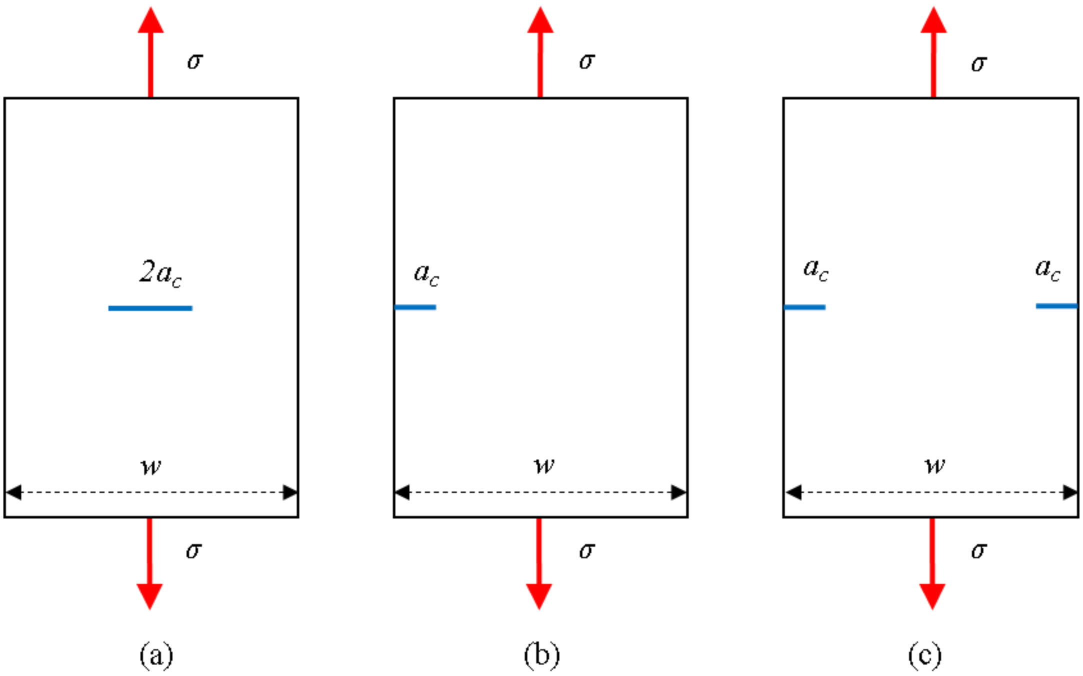

Fig. 14. Benchmark problems to compare with FEA results: (a) centred crack; (b) SENT; (c) DENT.

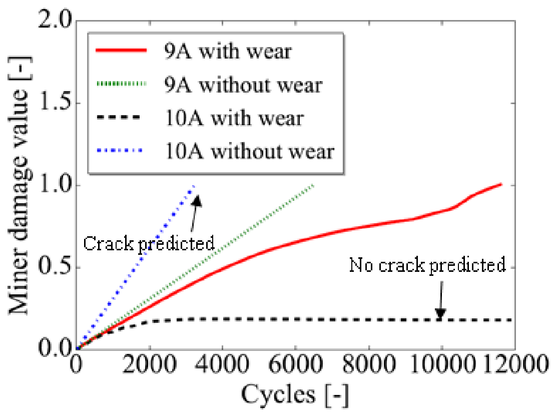

Fig. 15. Accumulated Miner's damage.

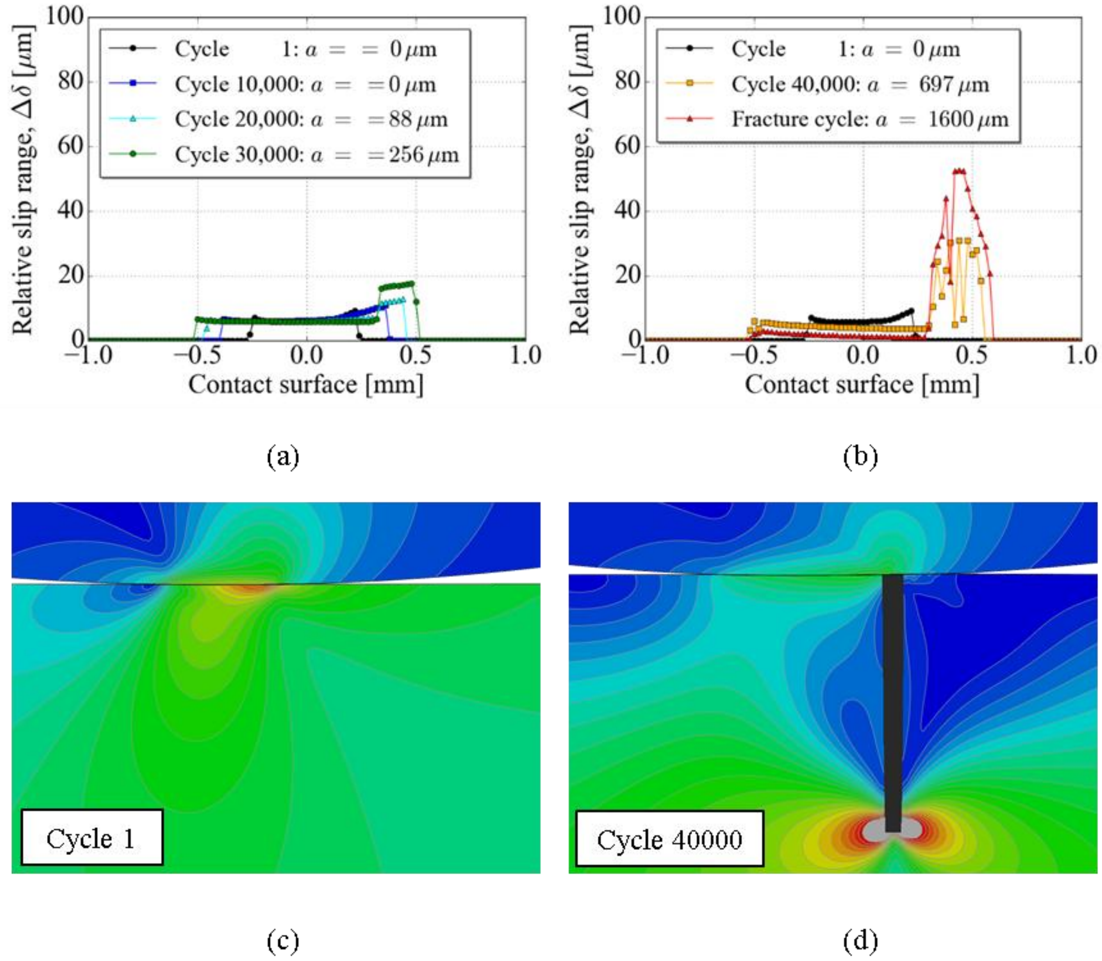

Fig. 16. Evolution of the contact relative slip and von Mises stress field at different stages of the simulation for test 9A: (a) relative slip up to 30,000 cycles; (b) relative slip at the final stages of the simulation; (c) VM stress field at the start of the simulation; (d) VM stress field at 40,000 cycles.

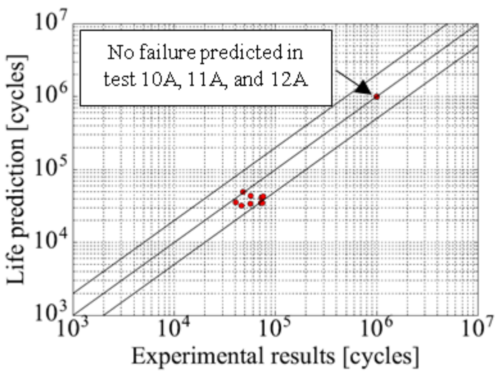

Fig. 17. Correlation between predicted and experimental lives.

Tables

Table 1. Experimental test summary [49].

Test	$D/2$ [mm]	P [N]	2Δ [µm]	N_f [cycles]
1A	50.08	4,003	54	71,843
2A	44.45	3,503	44	40,538
3A	38.10	3,003	34	46,129
4A	31.75	2,502	29	56,504
5A	25.40	2,002	27	74,288
6A	19.05	1,501	28	72,847
7A	15.24	1,201	33	56,992
8A	15.24	1,201	31	75,690
9A	12.7	1,001	36	47,833
10A	10.16	801	104	$>10^6$
11A	7.62	601	169	$>10^6$
12A	5.08	400	260	$>10^6$

Table 2. Calibration input parameters for the numerical simulation [18], [51]*, [52]**.

Yield strength	σ_y	930 MPa
Tensile strength	σ_u	1,100 MPa
Fatigue limit**	σ_0	300 MPa
Young's modulus	E	126 GPa
Poisson coefficient	υ	0.32
Fatigue strength coefficient*	$\sigma_f^{'}$	2,030 MPa
Basquin exponent*	b	-0.104
Fatigue ductility coefficient*	$\varepsilon_f^{'}$	0.841
Coffin-Manson exponent*	c	-0.688
Paris law coefficient	C	$1.25 \cdot 10^{-11}$ m/cycle/(MPa m$^{0.5}$)^m
Paris law exponent	m	2.59

SIF threshold	K_{th}	4.2 MPa $m^{1/2}$
Fracture toughness**	K_{IC}	90 MPa $m^{1/2}$
Coefficient of friction	μ	0.8
Wear coefficient	k	$2.75 \cdot 10^{-8}$ mm^3/N mm

Table 3. Comparison between weight function method and FEA for different crack benchmark problems.

	$K_{\text{I,WF}}$	$K_{\text{I,X-FEM}}$	***diff***
	$\text{MPa}\sqrt{\text{mm}}$	$\text{MPa}\sqrt{\text{mm}}$	*%*
Centred crack	**1.842**	**1.841**	**0.032**
SENT	**1.653**	**1.653**	**0.013**
DENT	**1.996**	**1.993**	**0.152**

Table 4. Comparison between predicted lifetime N_f and experimental result (Exp. N_f). Error is presented as a percentage change with respect to the experimental N_f.

Test	**Num.** N_i **[Cycles]**	**Num.** N_p **[Cycles]**	**Num.** N_f **[Cycles]**	**Exp.** N_f **[Cycles]**	**Error [%]**
1A	10,400	24,500	34,900	71,843	51.4
2A	10,500	25,000	35,500	40,538	12.4
3A	8,000	24,000	32,000	46,129	30.6
4A	6,800	27,200	34,000	56,504	39.8
5A	7,200	27,600	34,800	74,288	53.2
6A	8,000	33,200	41,200	72,847	43.4
7A	10,400	33,200	43,600	56,992	23.5
8A	10,000	32,800	42,800	75,690	43.4
9A	11,400	38,000	49,400	47,833	3.3
10A	Not predicted	-	Not predicted	$>10^6$	0
11A	Not predicted	-	Not predicted	$>10^6$	0
12A	Not predicted	-	Not predicted	$>10^6$	0